Article:
Jiang, Z., Chen, H., Liu, W. et al. (2022) 3-D temporal-spatial-based near-field source localization considering amplitude attenuation. Signal Processing, 201. 108735. ISSN: 0165-1684

https://doi.org/10.1016/j.sigpro.2022.108735

3-D Temporal-spatial-based Near-Field Source Localization Considering Amplitude Attenuation

Zhiwei Jiang[a], Hua Chen[a,b,*], Wei Liu[c], Gang Wang[a]

[a]*Faculty of Electrical Engineering and Computer Science, Ningbo University, Ningbo 315211, P. R. China.*
[b]*Key Laboratory of Intelligent Perception and Advanced Control of State Ethnic Affairs Commission, Dalian 116600, China.*
[c]*Department of Electronic and Electrical Engineering, University of Sheffield, Sheffield S1 3JD, UK.*

Abstract

A three-dimensional (3-D) localization algorithm for multiple near-field (NF) sources considering amplitude attenuation is proposed in this paper. Firstly, we use the symmetry of the array and the delay autocorrelation of NF signals to construct the virtual received data, whose phase factor is linear with the sensor position. By using the symmetry of amplitude attenuation of the virtual received data, a one-dimensional (1-D) peak search estimator is constructed to obtain the first angle parameter. Then, the estimated result is substituted into another spectral peak search function based on the original data to estimate the range parameter. Finally, a single-snapshot virtual received data set is generated, and the remaining angle parameter is solved by a phase retrieval operation. The proposed algorithm can automatically match the 3-D parameters, and has a stable estimation performance

*Corresponding author
Email addresses: dkchenhua0714@hotmail.com (Hua Chen), w.liu@sheffield.ac.uk (Wei Liu), wanggang@nbu.edu.cn (Gang Wang)

considering amplitude attenuation, as demonstrated by simulation results.
Keywords: Source localization, near-field sources, amplitude attenuation, temporal-spatial.

---

1. Introduction

As an important topic in source localization, the case with near-field (NF) sources has found many applications in radar [1] and wireless communications [2]. With the source-sensor distance being within the Rayleigh distance (known as in the Fresnel region) of the array [3], the wavefront curvature becomes spherical, where direction-of-arrival (DOA) and range of the NF sources need to be jointly estimated. A series of NF source localization methods have been proposed, including the subspace methods [4–6], and the sparse representation methods [7], where only the one-dimensional (1-D) angle (azimuth) and range can be obtained based on linear arrays. For the more general case, i.e., three-dimensional (3-D) estimation, where the parameters of interest are elevation, azimuth and range, two typical solutions can be found in [8] and [9], which are based on a center-symmetric cross array, employing the subspace rotation invariance method and optimization method, respectively. Unfortunately, all above-mentioned algorithms ignore amplitude attenuation of the received signal, which varies from sensor to sensor and is inversely proportional to the source-sensor distance, as pointed out in [10, 11]. Such a mismatch of the NF source model with physical reality will no doubt lead to performance degradation in parameter estimation.

On the other hand, it is important to exploit the spatial and temporal information in the process to improve the parameter estimation performance

[12]. Based on fourth-order cumulants, a 3-D subspace rotational invariance algorithm is proposed in [13], which transforms the NF data into virtual temporal-spatial far-field (FF) pseudo-data (a source beyond the Rayleigh distance of the array is considered a far-field (FF) source, whose wavefront is planar) by selecting specific array elements in two subarrays of the cross array. Subsequently, another 3-D NF localization method is proposed in [14] by constructing a set of temporal-spatial domain correlation matrices, which reduces the computational complexity by avoiding the calculation of cumulants. However, a parameter pairing process is required in [13, 14], which may cause pairing errors in some unfavorable conditions. Then, a 3-D parameter estimation method with automatic pairing is proposed in [15], where it first constructs a conjugate augmented spatial-temporal cross correlation matrix, and then three 1-D peak searches are performed to obtain estimates of the 3-D parameters, which is also applicable to the underdetermined scenario. However, one common issue with the above methods is that no amplitude attenuation is considered in their models.

In this paper, a spatial-temporal 3-D localization method for NF sources considering amplitude attenuation is proposed. We first use the spatial-temporal characteristics of the array received data and the symmetry of the array structure to obtain the virtual received data whose phase factor is linear with the sensor position, and then the two 1-D peak search estimators are constructed to find one angle and the range parameters, while the other angle parameter is estimated by phase retrieval. This method can realize automatic pairing of 3-D parameters, and a satisfactory estimation performance is achieved as demonstrated by computer simulations.

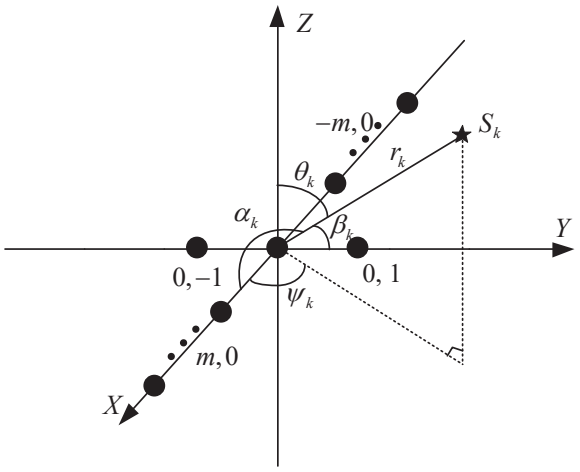

Figure 1: Geometry of a cross array for NF source localization.

Notations: Matrices and vectors are denoted by boldfaced capital letters and lower-case letters, respectively. $\|\cdot\|$ denotes the l_2-norm of a vector. The superscript $(\cdot)^T$, $(\cdot)^*$, $(\cdot)^H$ stand for transpose, conjugate and conjugate transpose, respectively. The notations $E\{\cdot\}$, $\delta(\cdot)$, $\det[\cdot]$ represent the expectation, Dirac function, and determinant, respectively. $pinv(\cdot)$ denotes the pseudo inverse of the matrix, $angle(\cdot)$ denotes the phase-taking operation, and $\max\{\cdot\}$ represents the maximum value.

2. Signal Model

As shown in Fig. 1, the cross array considered in our work is composed of two symmetrical uniform subarrays. The centers of symmetry of the two subarrays are located at the same point, i.e., the origin of the coordinate system. The sensor at the origin is shared by the two subarrays, and utilized as the amplitude and phase reference point. The subarray located on the x-axis is denoted as subarray x, whose number of sensors on one side of

the origin is N_x, with the total number of sensors in the subarray being $M_x = 2N_x + 1$; the subarray located on the y-axis is denoted as subarray y, which has only three sensors, one for each side. The inter-element spacing of each subarray is d, which is taken as the unit length of the coordinate system. There are K narrowband NF sources impinging onto the array from angles and ranges $(\theta_1, \varphi_1, r_1), \cdots, (\theta_k, \varphi_k, r_k), \cdots, (\theta_K, \varphi_K, r_K)$, $k = 1, 2, \cdots, K$, where θ_k and φ_k denote the elevation and azimuth angles of the k-th signal, respectively, and r_k denotes the range from the k-th source to the reference sensor. Moreover, α_k and β_k in Fig. 1 denote the angles between direction of the k-th signal and x- and y-axes, respectively. According to geometric structure of the array, α_k and β_k are related to azimuth and elevation angles by,

$$\begin{aligned} \cos(\alpha_k) &= \sin(\theta_k)\cos(\varphi_k) \\ \sin(\beta_k) &= \sin(\theta_k)\sin(\varphi_k). \end{aligned} \tag{1}$$

Utilizing the relationship in Eq. (1), the range from the source to the sensor located at coordinates $(m, 0)$ or $(0, n)$ ($m \in \{-N_x, \cdots, 0, \cdots, N_x\}, n \in \{-1, 0, 1\}$) can be written as

$$\begin{aligned} r_{m,k} &= \begin{cases} \sqrt{r_k^2 + (md)^2 - 2r_k md\cos\alpha_k}, m > 0 \\ \sqrt{r_k^2 + (md)^2 + 2r_k md\cos\alpha_k}, m \le 0 \end{cases} \\ r_{n,k} &= \begin{cases} \sqrt{r_k^2 + (nd)^2 - 2r_k nd\cos\beta_k}, n > 0 \\ \sqrt{r_k^2 + (nd)^2 + 2r_k nd\cos\beta_k}, n \le 0. \end{cases} \end{aligned} \tag{2}$$

Based on the assumption of narrowband signal, the propagation delays of the signals can be converted into phase shifts, so the output of the sensor

located at coordinates $(m, 0)$ or $(0, n)$ can be written as follows [10, 11]

$$\begin{aligned} x_m(t) &= \sum_{k=1}^{K} \left(\frac{r_k}{r_{m,k}}\right)^{\frac{p}{2}} e^{-j\frac{2\pi}{\lambda}(r_{m,k}-r_k)} s_k(t) + w_m(t) \\ &= \sum_{k=1}^{K} \gamma_{m,k} e^{-j\frac{2\pi}{\lambda}(r_{m,k}-r_k)} s_k(t) + w_m(t) \\ y_n(t) &= \sum_{k=1}^{K} \left(\frac{r_k}{r_{n,k}}\right)^{\frac{p}{2}} e^{-j\frac{2\pi}{\lambda}(r_{n,k}-r_k)} s_k(t) + w_n(t) \\ &= \sum_{k=1}^{K} \gamma_{n,k} e^{-j\frac{2\pi}{\lambda}(r_{n,k}-r_k)} s_k(t) + w_n(t), \end{aligned} \tag{3}$$

where $\gamma_{m,k} = \left(\frac{r_k}{r_{m,k}}\right)^{\frac{p}{2}}, \gamma_{n,k} = \left(\frac{r_k}{r_{n,k}}\right)^{\frac{p}{2}}$ denote the amplitude attenuation, λ is the wavelength of the signals and p denotes the prior known path-loss attenuation exponent value; $w_m(t)$ and $w_n(t)$ denote the additive noise on the corresponding sensor of each subarray. To simplify the model, Fresnel approximation to the phase delay is adopted [4–6], where the array output can be rewritten as

$$\begin{aligned} x_m(t) &= \sum_{k=1}^{K} \left(\frac{r_k}{r_{m,k}}\right)^{\frac{p}{2}} e^{-j(m\omega_{xk}+m^2\mu_{xk})} s_k(t) + w_m(t) \\ &= \sum_{k=1}^{K} a_m(\alpha_k, r_k) s_k(t) + w_m(t) \\ y_n(t) &= \sum_{k=1}^{K} \left(\frac{r_k}{r_{n,k}}\right)^{\frac{p}{2}} e^{-j(n\omega_{yk}+n^2\mu_{yk})} s_k(t) + w_n(t) \\ &= \sum_{k=1}^{K} a_n(\beta_k, r_k) s_k(t) + w_n(t), \end{aligned} \tag{4}$$

where

$$\begin{aligned} \omega_{xk} &= -\tfrac{2\pi d}{\lambda}\cos\alpha_k, \mu_{xk} = \tfrac{\pi d^2}{\lambda r_k}\sin^2\alpha_k, \\ \omega_{yk} &= -\tfrac{2\pi d}{\lambda}\cos\beta_k, \mu_{yk} = \tfrac{\pi d^2}{\lambda r_k}\sin^2\beta_k. \end{aligned} \tag{5}$$

Then, the data vector collected by the subarray x or y at time t can be

expressed compactly as

$$\begin{aligned}\mathbf{x}(t) &= \sum_{k=1}^{K} \mathbf{a}_x(\alpha_k, r_k) s_k(t) + \mathbf{w}_x(t) = \mathbf{A}_x \mathbf{s}(t) + \mathbf{w}_x(t) \\ \mathbf{y}(t) &= \sum_{k=1}^{K} \mathbf{a}_y(\beta_k, r_k) s_k(t) + \mathbf{w}_y(t) = \mathbf{A}_y \mathbf{s}(t) + \mathbf{w}_y(t),\end{aligned} \tag{6}$$

where $\mathbf{A}_x = [\mathbf{a}_x(\alpha_1, r_1), ..., \mathbf{a}_x(\alpha_k, r_k), ..., \mathbf{a}_x(\alpha_K, r_K)]^T$ with $\mathbf{a}_x(\alpha_k, r_k) = [a_{-N_x}(\alpha_k, r_k), ..., a_m(\alpha_k, r_k) ..., a_{N_x}(\alpha_k, r_k)]^T$ denotes the $M_x \times K$ manifold matrix of subarray x, $\mathbf{A}_y$ is similarly defined, $\mathbf{s}(t) = [s_1(t), \cdots, s_K(t)]^T$ denotes the $K \times 1$ baseband signal vector, and $\mathbf{w}_x(t)$ and $\mathbf{w}_y(t)$ are the corresponding noise vectors.

As θ_k and φ_k can be determined when α_k and β_k are retrieved, the objective of the proposed algorithm in this paper is to estimate the group of angle-range $(\theta_k, \varphi_k, r_k)$ from N snapshots of data collected by the cross array. Unless otherwise specified, the following assumptions are made for the proposed method,

1) The sensor spacing should satisfy $d \leq \frac{\lambda}{4}$ to avoid angular ambiguity;

2) The number of sources K is known or can be estimated by some well-known methods [16, 17], and the source signals are not correlated with each other;

3) The noise is additive white Gaussian and independent of the signals.

3. Proposed Method

3.1. Estimate α_k, r_k

As observed from Eq. (4), the phase factor of the NF sources contains a linear term and a quadratic term, and the coefficient ω_{xk} of the linear term contains only one estimated parameter α. Accordingly, we utilize the

symmetry of the array and the delay autocorrelation of the signal to construct the following virtual received data,

$$\begin{aligned} r_{m,-m}(\tau) &= E\{x_m(t+\tau)\, x_{-m}^*(t)\} \\ &= \sum_{k=1}^{K} \gamma_{m,k}\gamma_{-m,k} e^{-j\left(m\omega_{xk}+m^2\mu_{xk}\right)} e^{-j\left((-m)\omega_{xk}+(-m)^2\mu_{xk}\right)} \\ &\quad \times E\{s_k(t+\tau)\, s_k(t)\} + \sigma_\omega^2 \delta(m)\,\delta(\tau) \\ &= \sum_{k=1}^{K} \tilde{\gamma}_{m,k} e^{-j2m\omega_{xk}} r_{sk}(\tau) + \sigma_\omega^2 \delta(m)\,\delta(\tau), \end{aligned} \tag{7}$$

where $\tilde{\gamma}_{m,k} = \gamma_{m,k}\gamma_{-m,k}$ denotes the amplitude attenuation of virtual received data and σ_ω^2 is noise power, and $r_{sk}(\tau) = E\{s_k(t+\tau)\, s_k(t)\}$ denotes the delay autocorrelation of the k-th signal. Concatenating $r_{m,-m}(\tau)$ for $m = -N_x, \cdots, 0, \cdots, N_x$, a vector of size $M_x \times 1$ is constructed as follows,

$$\mathbf{r}_1(\tau) = [r_{-N_x,N_x}(\tau), \cdots, r_{0,0}(\tau), \cdots, r_{N_x,-N_x}(\tau)]^T, \tag{8}$$

or alternatively

$$\mathbf{r}_1(\tau) = \mathbf{A}_1 \mathbf{r}_s(\tau), \tag{9}$$

where

$$\mathbf{A}_1 = [\mathbf{a}_1(\alpha_1, r_1), \cdots, \mathbf{a}_1(\alpha_k, r_k), \cdots, \mathbf{a}_1(\alpha_K, r_K)],$$

$$\mathbf{a}_1(\alpha_k, r_k) = \left[\tilde{\gamma}_{-N_x,k} e^{-j2(-N_x)\omega_{xk}}, \cdots, 1, \cdots, \tilde{\gamma}_{N_x,k} e^{-j2N_x\omega_{xk}}\right]^T,$$

$$\mathbf{r}_s(\tau) = [r_{s1}(\tau), \cdots, r_{sK}(\tau)]^T.$$

By uniformly sampling $\mathbf{r}_1(\tau)$ at $L(L > M_x)$ lags $\tau_l(\tau_l = T_s, 2T_s, \cdots, LT_s)$, the "pseudo snapshots" matrix can be collected as follows,

$$\mathbf{R}_1 = [\mathbf{r}_1(T_s), \mathbf{r}_1(2T_s), \cdots, \mathbf{r}_1(LT_s)] = \mathbf{A}_1 \mathbf{R}_s \tag{10}$$

where $\mathbf{R}_s = [\mathbf{r}_s(T_s), \cdots, \mathbf{r}_s(LT_s)]$ denotes the delay autocorrelation matrix of the signal.

Calculate the covariance matrix of the virtual received data $\mathbf{R}_1$ in Eq. (10), and then perform eigenvalue decomposition (EVD) to obtain

$$\tilde{\mathbf{R}}_1 = E\left\{\mathbf{R}_1\mathbf{R}_1^H\right\} = \mathbf{U}_S\mathbf{\Sigma}_S\mathbf{U}_S^H + \mathbf{U}_N\mathbf{\Sigma}_N\mathbf{U}_N^H \tag{11}$$

where $\mathbf{\Sigma}_S$ denotes a diagonal matrix containing K largest eigenvalues, whose corresponding eigenvectors for the signal subspace $\mathbf{U}_S$, while $\mathbf{\Sigma}_N$ contains the $M_x - K$ smallest eigenvalues on its diagonal and $\mathbf{U}_N$ denotes the corresponding noise subspace. Based on the orthogonality principle [15], the following spectral peak estimator can be constructed

$$f_1(\alpha, r) = [\mathbf{a}_1^H(\alpha, r)\,\mathbf{U}_N^H\mathbf{U}_N\mathbf{a}_1(\alpha, r)]^{-1}. \tag{12}$$

It can be seen from Eq. (12) that the above spectral peak function has two estimated parameters, which could be solved directly by the time-consuming two-dimensional (2-D) search method. In order to reduce the computational complexity, a series of preprocessing operations are applied to the function $f_1(\alpha, r)$.

According to Eqs. (2) and (7), we have

$$\tilde{\gamma}_{-m,k} = \tilde{\gamma}_{m,k}, \tag{13}$$

and therefore, $\mathbf{a}_1(\alpha, r)$ can be written as

$$\mathbf{a}_1(\alpha, r) = \begin{bmatrix} e^{-j2(-N_x)\omega_x} & & & & \\ & e^{-j2(-N_x+1)\omega_x} & & & \\ & & \ddots & & \\ & & & 1 & \\ & & & \iddots & \\ & & e^{-j2(N_x-1)\omega_x} & & \\ e^{-j2N_x\omega_x} & & & & \end{bmatrix} \begin{bmatrix} \tilde{\gamma}_{-N_x} \\ \tilde{\gamma}_{-N_x+1} \\ \vdots \\ \tilde{\gamma}_{-1} \\ 1 \end{bmatrix} = \boldsymbol{\zeta}(\alpha)\, \boldsymbol{\upsilon}(\alpha, r). \tag{14}$$

It can be seen that $\boldsymbol{\upsilon}(\alpha, r) \neq 0$ from Eq. (14), and then by utilizing the rank-reduction principle [18–20], we can obtain a spectral peak function only related to angle α as follows,

$$P(\alpha) = [\det(\boldsymbol{\zeta}^H(\alpha)\, \mathbf{U}_N^H \mathbf{U}_N \boldsymbol{\zeta}(\alpha))]^{-1}. \tag{15}$$

After obtaining the estimated value $\hat{\alpha}$ from Eq. (15), we proceed to estimate the range parameter. Although the virtual received data constructed in Eq. (10) contains the range parameter, it only appears in the amplitude attenuation part, whose estimation performance might not be as good as that from the phase factor. Therefore, the original received data of subarray x in Eq. (6) is considered, and by performing EVD on covariance matrix of Eq. (6), we have the noise subspace $\mathbf{U}'_N$. Applying the orthogonality principle again, the following 1-D spectral peak function can be obtained

$$P'(\hat{\alpha}, r) = [\mathbf{a}_x^H(\hat{\alpha}, r) \mathbf{U}'^H_N \mathbf{U}'_N \mathbf{a}_x(\hat{\alpha}, r)]^{-1}. \tag{16}$$

Thus, estimation of the range parameter $\hat{r}$ is achieved from Eq. (16) by resorting to the estimated value $\hat{\alpha}$ from Eq. (15).

3.2. Discrimination of pseudo peaks

As pointed out in Ref. [20], rank-reduction methods might yield serious pseudo peaks, resulting in ambiguous DOA estimates in some scenarios. Therefore, a true-peak selection method is developed as follows.

First, all the estimated values (including true peaks and pseudo peaks) obtained by Eq. (15) are substituted into Eq. (16) for range search. If there is an estimated angle value by which we cannot find the corresponding range value in the Fresnel area, the peak corresponding to that angle is then considered as a pseudo peak. It should be noted that pseudo peaks might still exist in the remaining peak values after the above operation. Next, several array steering matrices $\mathbf{B}_q(q = 1, 2, \cdots, C_P^K)$ are reconstructed by selecting K angle estimates corresponding to K peaks from the remaining P unrecognized peaks, which have C_P^K combinations. The combination of true peaks, which corresponds to unambiguous DOA estimates, is chosen by substituting C_P^K combinations to the following equation that minimizes the error in the least squares fitting

$$\mathbf{E}_q = \mathbf{R}_1 - \mathbf{B}_q \mathbf{R}_s. \tag{17}$$

Since $\mathbf{R}_s$ is not known a priori, the following error function e_q is constructed

$$e_q = \sum_{\tau} \left\| \mathbf{B}_q^{\perp} \mathbf{R}_1(:, \tau) \right\|^2, \tag{18}$$

where $\mathbf{B}_q^{\perp} = \mathbf{I} - \mathbf{B}_q(\mathbf{B}_q^H \mathbf{B}_q)^{-1} \mathbf{B}_q^H$ denotes the projection matrix onto the null space of $\mathbf{B}_q$. For each of the C_P^K combinations, e_q is calculated and the combination providing the minimum value is chosen as the true unambiguous

angle estimates. A summary of pseudo peak identification steps is shown in Table 1.

Table 1: Summary of Pseudo Peak Identification

Step 1 Perform EVD on $\mathbf{x}(n)$ to obtain $\mathbf{U}_n'$.
Step 2 Substitute the estimate $\hat{\alpha}$ corresponding to all peaks obtained by Eq. (15) into $P^{'}(\hat{\alpha}, r)$ of Eq. (16) for range search.
Step 3 Remove those angle estimates $\hat{\alpha}$ that are not able to provide the corresponding range parameters in the Fresnel area in **Step** 2.
Step 4 Select K values from the remaining P angle estimates for combination, and construct the corresponding steering matrix $\mathbf{B}_q(q = 1, 2, \cdots, C_P^K)$.
Step 5 Substitute $\mathbf{B}_q$ into Eq. (18) for calculation in turn, and the combination giving the minimum e_q is the true peaks.

3.3. Estimate β_k

Similar to Eq. (7), the virtual data related to subarray y is constructed as follows,

$$\begin{aligned} & r_{-1,1}(\tau) = E\{y_1(t+\tau)\, y_{-1}^*(t)\} \\ & = \sum_{k=1}^{K} \gamma_{1,k}\gamma_{-1,k} e^{-j\left(\omega_{yk}+\mu_{yk}\right)} e^{-j\left((-1)\omega_{yk}+(-1)^2\mu_{yk}\right)} E\{s_k(t+\tau)\, s_k(t)\} \\ & = \sum_{k=1}^{K} \bar{\gamma}_k e^{-j2\omega_{yk}} r_{sk}(\tau), \end{aligned} \tag{19}$$

where $\bar{\gamma}_k = \gamma_{1,k}\gamma_{-1,k}$ denotes the amplitude attenuation of structural data. By uniformly sampling $r_{-1,1}(\tau)$ at L lags $\tau_l(\tau_l = T_s, 2T_s, \cdots, LT_s)$, the "pseudo snapshots" can be collected as follows,

$$\mathbf{r}_2 = [r_{1,-1}(T_s), r_{1,-1}(2T_s), \cdots, r_{1,-1}(LT_s)] = \tilde{\mathbf{a}}\mathbf{R}_s, \tag{20}$$

where $\tilde{\mathbf{a}} = [\tilde{\gamma}_{y,1}e^{-j2\omega_{y1}}, ..., \tilde{\gamma}_{y,k}e^{-j2\omega_{yk}}, ..., \tilde{\gamma}_{y,K}e^{-j2\omega_{yK}}]$. Based on Eqs. (10) and (20), the following relationship can be attained,

$$\begin{aligned} \mathbf{r}_3 &= vec\left(E\left\{\mathbf{r}_2\mathbf{R}_1^H\right\}\right) \\ &= \mathbf{A}_1^*\mathbf{\Phi}\mathbf{r}_{ss}, \end{aligned} \tag{21}$$

where $\mathbf{\Phi} = diag\left(\tilde{\gamma}_{y,1}e^{-j2\omega_{y1}}, ..., \tilde{\gamma}_{y,k}e^{-j2\omega_{yk}}, ..., \tilde{\gamma}_{y,K}e^{-j2\omega_{yK}}\right)$, $\mathbf{r}_{ss} = [p_1, ..., p_k, ..., p_K]^T$, and p_k is the power of the k-th signal. Substituting the estimate of parameters $\hat{\alpha}, \hat{r}$ into Eq. (21) yields the following formula,

$$\mathbf{\Phi}\mathbf{r}_{ss} = pinv\left(\mathbf{A}_1^*\right)\mathbf{r}_3. \tag{22}$$

Since $\mathbf{r}_{ss}$ is a real vector, the estimated parameter $\hat{\beta}$ is given by

$$\hat{\beta} = a\cos\left(\frac{angle\left(\mathbf{\Phi}\mathbf{r}_{ss}\right)}{-2\pi d/\lambda}\right). \tag{23}$$

At this point, the 2-D DOA and range parameters are automatically paired without any additional operation. The proposed method is summarized in Table 2.

Remark 1: This method can be applied to non-uniform linear arrays, as long as they satisfy the symmetry property, which is exploited in the process of constructing the virtual receiving data.

Remark 2: In the purely near-field case, the angle estimation values that cannot be used for range search will be eliminated in the process of pseudo-peak recognition, and for the mixed case [21–24], the procedure for the pseudo-peak recognition needs to be modified in **step 3** of Table 1 as

Table 2: Summary of the proposed method.

Input: N snapshots of the two ULA output vectors: $\{\mathbf{x}(t), \mathbf{y}(t)\}_{n=1}^{N}$.
Output: 2-D DOA and range estimates of NF signals: $\hat{\alpha}_k$, $\hat{\beta}_k$ and $\hat{r}_k$.
Step 1 Construct $\mathbf{R_1}$ according to Eq. (10), where $\mathbf{r}_1(T_s), \mathbf{r}_1(2T_s), \cdots, \mathbf{r}_1(LT_s)$ are calculated by Eq. (7) and Eq. (8).
Step 2 Perform the EVD on $\mathbf{R_1}$ to obtain $\mathbf{U_n}$, and then construct and search through $P(\alpha)$ to obtain angles α_k with Eq. (15).
Step 3 Find the true peaks according to Table 1, and get the corresponding range estimate r_k with Eq. (16).
Step 4 Construct $\mathbf{r}_2$ with Eq. (20), and then calculate $\mathbf{r}_3$ through Eq. (21).
Step 5 Perform phase-taking operation on $\mathbf{r}_3$ to obtain the angle β_k with Eq. (23).

when some angle estimates cannot find the range parameter, the corresponding range estimate is set to ∞.

3.4. Complexity analysis

To facilitate analysis and comparison, the computational complexity of Chen's method in [15] and the proposed method is analyzed in this part. In the analysis, we only consider the parts with high complexity: covariance matrix calculation, eigenvalue decomposition, peak search and matrix inversion. Chen's method includes one covariance matrix calculation, one eigenvalue decomposition and three 1-D peak searches, while the proposed method involves two covariance matrix calculations, two eigenvalue decompositions, two 1-D peak searches and one matrix pseudo-inverse. A summary of the complexity of the two methods is shown in Table 3.

Table 3: Complexity comparison

Method	Complexity
Chen's method	$O\{36M_x^2(2L-1)+216M_x^3+n_\alpha(2M_x\cdot 8M_x(6M_x-K)$ $+n_\beta K((6M_x-K)\cdot 2(N_x+1)\cdot 2(M_x+N_x+1))$ $+n_r K((6M_x-K)(6M_x+1))\}$
Proposed method	$O\{M_x^2L+M_x^3+n_\alpha(M_x-K)(N_x+1)(M_x+N_x+1)$ $+n_r K(M_x-K)(M_x+1)+M_x^3\}$

4. Simulation and Results

The performance of the proposed method is compared with those in [9, 15] through numerical simulations. In all simulations, the source-to-sensor amplitude attenuation is assumed to follow the inverse-square law in physics, i.e., p=2. Moreover, as range estimation by the algorithms in [15] almost fails when amplitude attenuation is present, to better highlight the advantages of the proposed algorithm, the range search part of the algorithm in [9] is slightly modified to make it work. The array element spacing is $\frac{\lambda}{8}$, the total number of array elements is 9, and 500 Monte-Carlo trials are performed for all simulations.

The root mean square error (RMSE) versus signal-to-noise ratio (SNR) result is shown in Fig. 2, where the sources impinge onto the array from $\{60°, 135°, 0.8\lambda\}$ and $\{55°, 120°, 0.3\lambda\}$, and 2000 data snapshots are collected. The pseudo-snapshots of the proposed algorithm and those in Ref. [15] are both set to 50. The SNR varies from -5 dB to 25dB. It can be seen that with the increase of SNR, the performance of the proposed method has

significantly improved, while the compared methods tend to saturate, due to model mismatch without considering amplitude attenuation.

In Fig. 3, the performance is examined versus the number of snapshots. The settings are the same as in the first simulation, except that the SNR is 15dB and the number of snapshots is changed from 200 to 3500. Similar to the observation in Fig. 2, the change trend of the methods in [9] and [15] with respect to the number of snapshots is not obvious, i.e., it reaches a "saturated" state, while the proposed one still exhibits a good performance. In Fig. 3(c), Wu's method is modified so that the RMSE for range estimation decreases with increase of the number of snapshots.

In addition, the runtime of all three methods versus the number of snapshot is shown in Fig. 4. It can seen that the running time of the proposed algorithm is obviously shorter than that of Chen's method and Wu's method. This is because the dimension of the matrices constructed by the proposed method is smaller than that of Chen's method, and it is search-free for the third parameter. As compared with Wu's method, the proposed algorithm avoids the calculation of the fourth-order cumulant, and thus the computational complexity is effectively reduced.

Then, the angle resolution of the proposed method is studied. The resolution performance is presented by the estimated success rate under the same condition, and the success criterion is given below.

$$\max\left\{\max_{k=1,2,\cdots,K}\left|\alpha_k-\hat{\alpha}_k\right|,\max_{k=1,2,\cdots,K}\left|\beta_k-\hat{\beta}_k\right|\right\}\leq\varepsilon, \tag{24}$$

where ε is the threshold for success and Fig. 5 shows the results when the threshold ε is 0.5°, 2° and 4°, respectively. Except for the 2-D angle parameters of the sources, the other configurations are the same as before.

The SNR is set to 15dB and the angle interval of 2-D DOAs simultaneously changes from 1° to 25°. From Fig. 5, we can see that with the increase of angle interval, the success rate of the compared methods stays at almost zero or increases only slightly. This is due to the significant error caused by ignoring amplitude attenuation. On the contrary, with the increase of angle interval, the success rate of the proposed method gradually increases.

Finally, we give an example to demonstrate the applicability of the proposed method for mixed NF and FF sources by setting the range of the second source and SNR to ∞ and 15dB, respectively in the first simulation, while keep other simulation parameters unchanged. From Fig. 6 (a), it can be seen that the proposed method has effectively identified the 2-D DOAs of the mixed sources, along with the range parameter of the first NF source in Fig. 6 (b).

5. Conclusions

In this work, the 3-D localization problem of NF sources has been studied considering the effect of amplitude attenuation. By exploiting the temporal-spatial information of the received data, the proposed method has three stages for pairing-free estimation of the 3-D parameters and enjoys a higher estimation accuracy either in 2-D DOAs or range estimation than two existing methods, as demonstrated by computer simulations. To distinguish pseudo and true peaks occasionally caused by the rank-reduction method, a procedure is introduced for the method to reach an unambiguous estimation result.

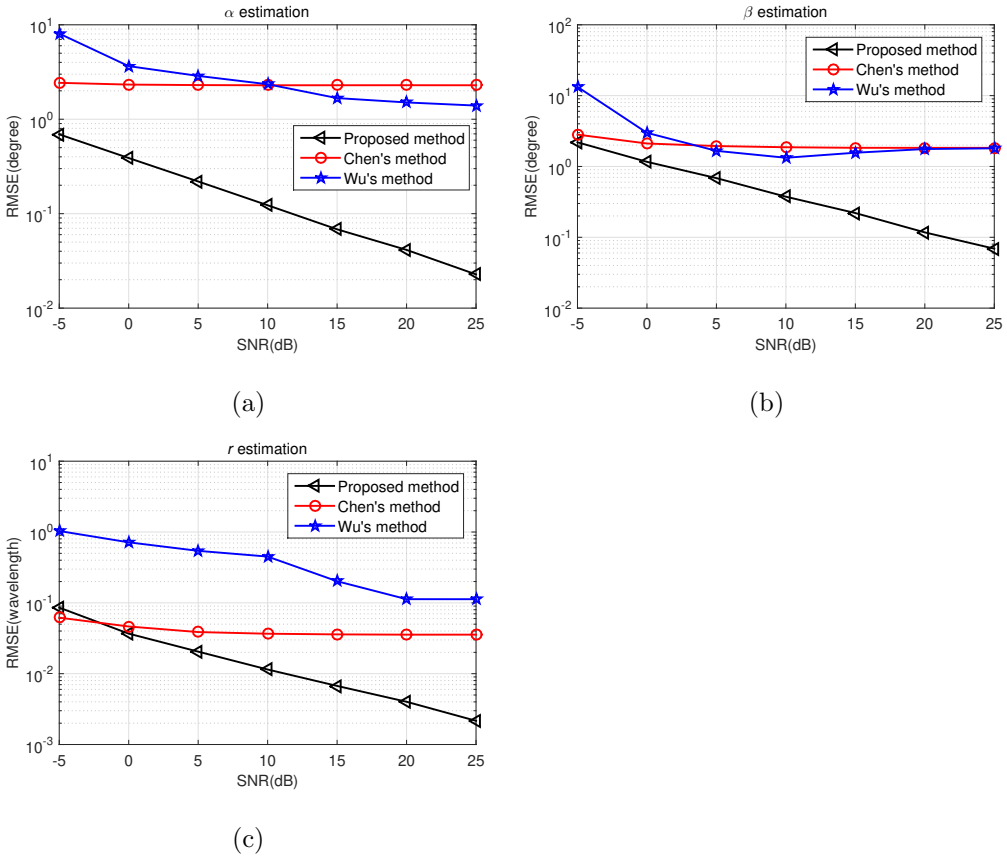

Figure 2: RMSEs versus SNR.

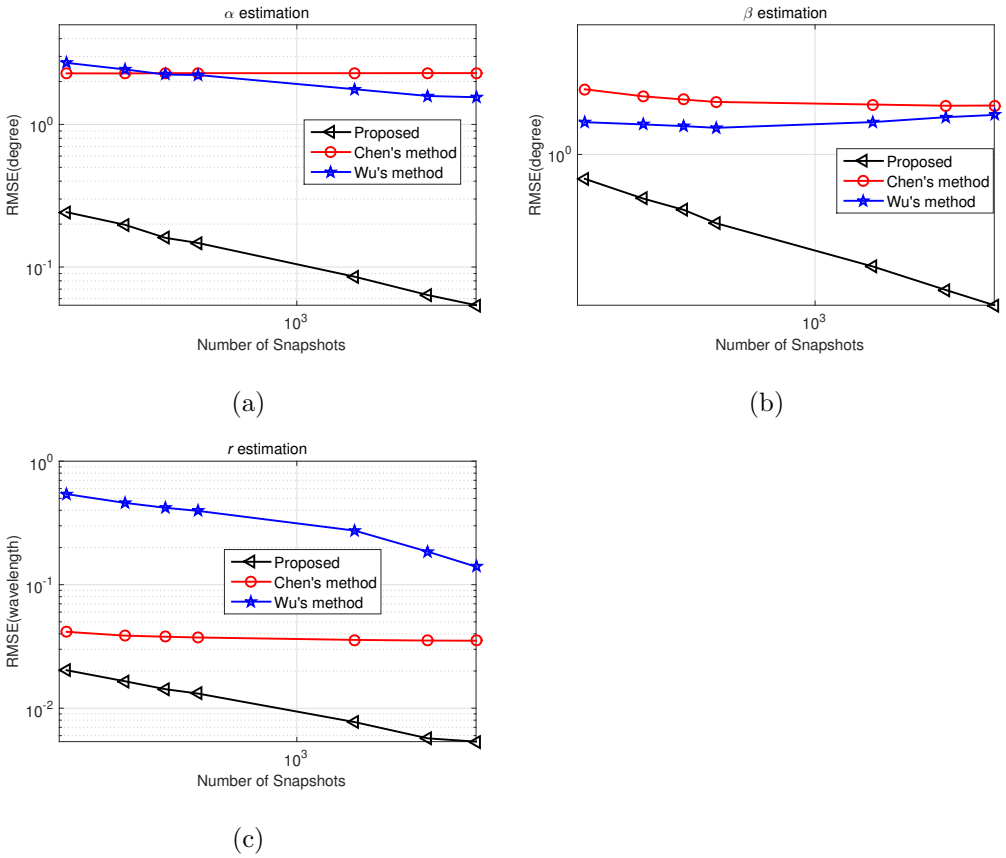

Figure 3: RMSEs versus the number of snapshots.

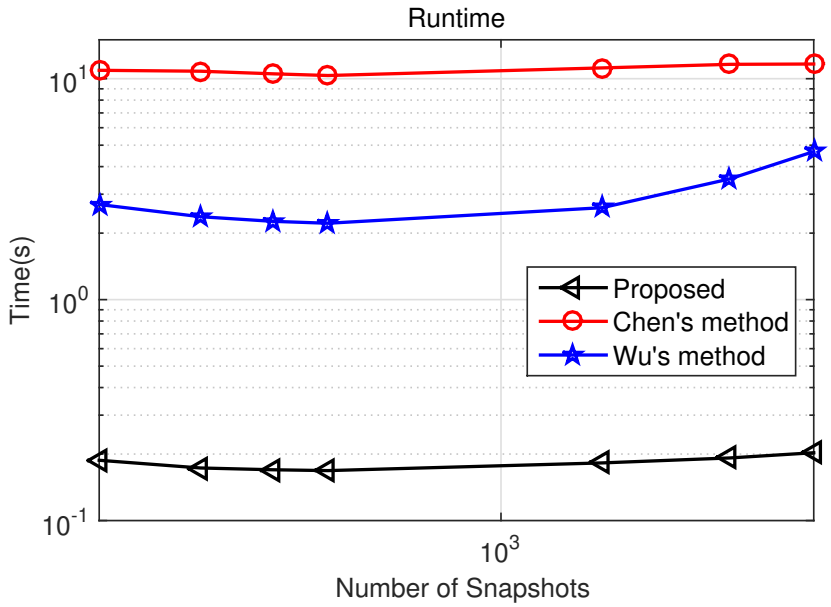

Figure 4: Runtime versus the number of snapshots

Acknowledgement

This work was supported by the National Natural Science Foundation of China under grants 62001256 and 62222109, and by Key Laboratory of Intelligent Perception and Advanced Control of State Ethnic Affairs Commission under grant MD-IPAC-2019102, and by Zhejiang Provincial Natural Science Foundation of China under grant LR20F010001, and the UK Engineering and Physical Sciences Research Council (EPSRC) under grants EP/T517215/1 and EP/V009419/1, and by the Scientific Research Foundation of Graduate School of Ningbo University under grant IF2022130.

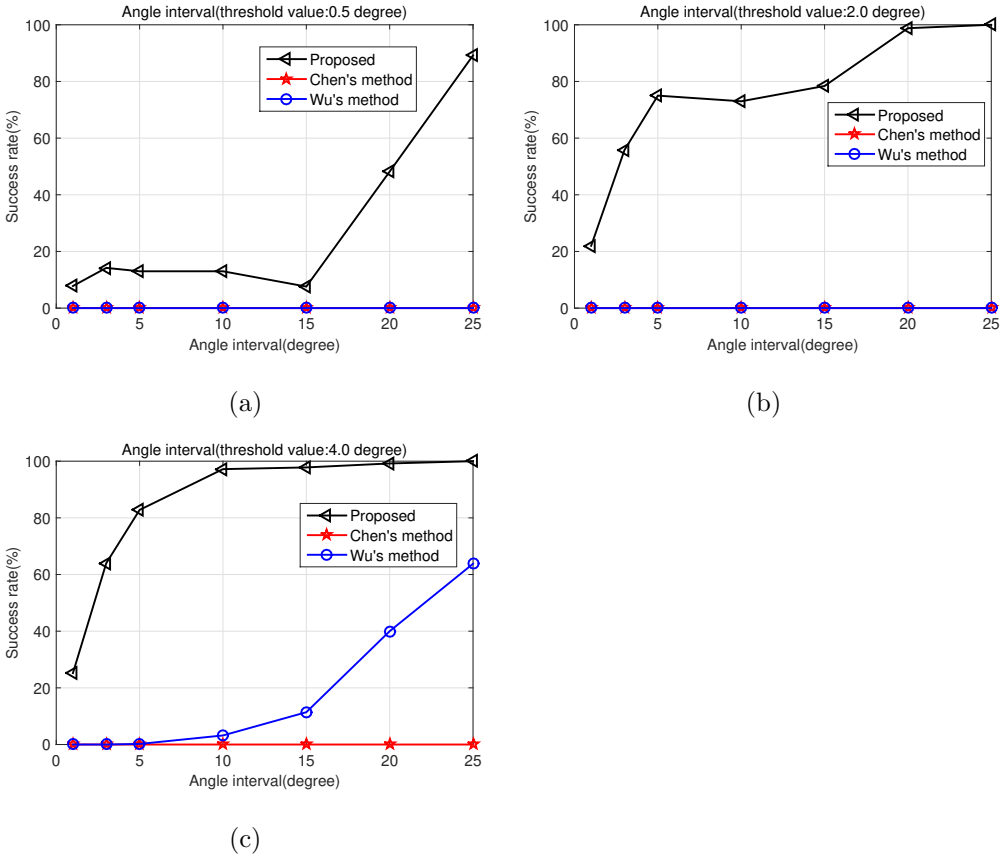

Figure 5: Success rate versus angle interval.

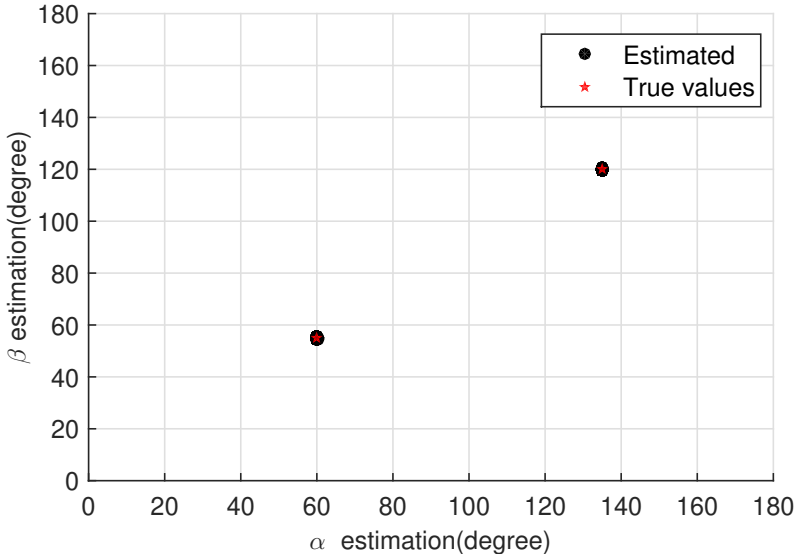

(a) 2-D DOAs

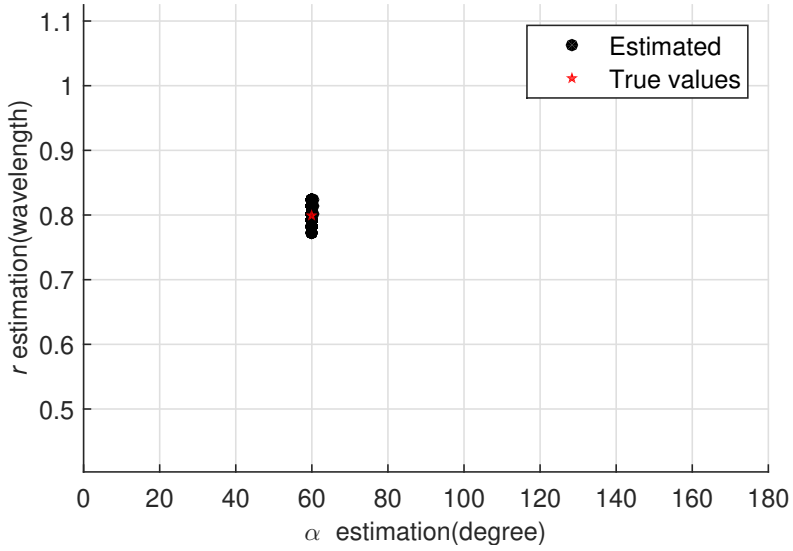

(b) DOA and Range

Figure 6: Scatter diagram of mixed sources.

References

[1] A. Sakhnini, S. De Bast, M. Guenach, A. Bourdoux, H. Sahli, S. Pollin, Near-field coherent radar sensing using a massive MIMO communication testbed, IEEE Transactions on Wireless Communications (2022) 1–1doi:10.1109/TWC.2022.3148035.

[2] Y. Cao, T. Lv, Z. Lin, P. Huang, F. Lin, Complex resnet aided DoA estimation for near-field MIMO systems, IEEE Transactions on Vehicular Technology 69 (10) (2020) 11139–11151. doi:10.1109/TVT.2020.3007894.

[3] J. He, T. Shu, L. Li, T.-K. Truong, Mixed near-field and far-field localization and array calibration with partly calibrated arrays, IEEE Transactions on Signal Processing 70 (2022) 2105–2118. doi:10.1109/TSP.2022.3168975.

[4] Z. Zheng, M. Fu, W. Q. Wang, H. C. So, Mixed far-field and near-field source localization based on subarray cross-cumulant, Signal Processing 150 (2018) 51–56.

[5] H. Chen, W. Wang, W. Liu, Joint DOA, range, and polarization estimation for rectilinear sources with a COLD array, IEEE Wireless Communications Letters 8 (5) (2019) 1398–1401. doi:10.1109/LWC.2019.2919542.

[6] Z. Zheng, M. Fu, W.-Q. Wang, S. Zhang, Y. Liao, Localization of mixed near-field and far-field sources using symmetric double-nested arrays, IEEE Transactions on Antennas and Propagation 67 (11) (2019) 7059–7070. doi:10.1109/TAP.2019.2925199.

[7] L. Yang, J. Li, F. Chen, Y. Wei, F. Ji, H. Yu, Localization of incoherently distributed near-field sources: A low-rank matrix recovery approach, Signal Processing 189 (2021) 108273. doi:https://doi.org/10.1016/j.sigpro.2021.108273.

[8] K. Abed-Meraim, Y. Hua, 3-D near field source localization using second order statistics, in: Conference Record of the Thirty-First Asilomar Conference on Signals, Systems and Computers (Cat. No.97CB36136), Vol. 2, 1997, pp. 1307–1311 vol.2. doi:10.1109/ACSSC.1997.679115.

[9] X. Wu, J. Yan, 3-D mixed far-field and near-field sources localization with cross array, IEEE Transactions on Vehicular Technology 69 (6) (2020) 6833–6837. doi:10.1109/TVT.2020.2985903.

[10] B. Friedlander, Localization of signals in the near-field of an antenna array, IEEE Transactions on Signal Processing 67 (15) (2019) 3885–3893. doi:10.1109/TSP.2019.2923164.

[11] J. He, L. Li, T. Shu, T.-K. Truong, Mixed near-field and far-field source localization based on exact spatial propagation geometry, IEEE Transactions on Vehicular Technology 70 (4) (2021) 3540–3551. doi:10.1109/TVT.2021.3065954.

[12] F. Wen, P. Liu, H. Wei, Y. Zhang, R. C. Qiu, Joint azimuth, elevation, and delay estimation for 3-D indoor localization, IEEE Transactions on Vehicular Technology 67 (5) (2018) 4248–4261. doi:10.1109/TVT.2018.2794322.

[13] R. N. Challa, S. Shamsunder, Passive near-field localization of multiple non-gaussian sources in 3-D using cumulants, Signal Processing 65 (1) (1998) 39–53. doi:https://doi.org/10.1016/S0165-1684(97)00206-5.

[14] K. Deng, Q. Yin, Closed form parameters estimation for 3-D near field sources 4 (2006) IV–IV. doi:10.1109/ICASSP.2006.1661173.

[15] H. Chen, Z. Jiang, W. Liu, Y. Tian, G. Wang, Conjugate augmented decoupled 3-D parameters estimation method for near-field sources, IEEE Transactions on Aerospace and Electronic Systems (2022) 1–1doi:10.1109/TAES.2022.3164864.

[16] L. Huang, C. Qian, H. Cheung So, J. Fang, Source enumeration for large array using shrinkage-based detectors with small samples, IEEE Transactions on Aerospace and Electronic Systems 51 (1) (2015) 344–357. doi:10.1109/TAES.2014.130579.

[17] L. Huang, T. Long, E. Mao, H. C. So, MMSE-based MDL method for robust estimation of number of sources without eigendecomposition, IEEE Transactions on Signal Processing 57 (10) (2009) 4135–4142. doi:10.1109/TSP.2009.2024043.

[18] M. Pesavento, A. B. Gershman, K. M. Wong, On uniqueness of direction of arrival estimates using rank reduction estimator (RARE), in: 2002 IEEE International Conference on Acoustics, Speech, and Signal Processing, Vol. 3, 2002, pp. III–3021–III–3024. doi:10.1109/ICASSP.2002.5745285.

[19] M. Pesavento, C. Mecklenbrauker, J. Bohme, Multidimensional rank reduction estimator for parametric MIMO channel models, Eurasip Journal on Advances in Signal Processing 2004 (9) (2004) 1–10.

[20] J. Dai, X. Bao, N. Hu, C. Chang, W. Xu, A recursive rare algorithm for DOA estimation with unknown mutual coupling, IEEE Antennas and Wireless Propagation Letters 13 (2014) 1593–1596. doi:10.1109/LAWP.2014.2347056.

[21] W. Zuo, J. Xin, W. Liu, N. Zheng, H. Ohmori, A. Sano, Localization of near-field sources based on linear prediction and oblique projection operator, IEEE Transactions on Signal Processing 67 (2) (2019) 415–430. doi:10.1109/TSP.2018.2883034.

[22] H. Chen, W.-P. Zhu, W. Liu, M. Swamy, Y. Li, Q. Wang, Z. Peng, Rare-based localization for mixed near-field and far-field rectilinear sources, Digital Signal Processing 85 (2019) 54–61. doi:https://doi.org/10.1016/j.dsp.2018.11.006.

[23] Z. Zheng, M. Fu, W.-Q. Wang, H. C. So, Symmetric displaced coprime array configurations for mixed near- and far-field source localization, IEEE Transactions on Antennas and Propagation 69 (1) (2021) 465–477. doi:10.1109/TAP.2020.3005203.

[24] X. Su, P. Hu, Z. Liu, T. Liu, B. Peng, X. Li, Mixed near-field and far-field source localization based on convolution neural networks via symmetric nested array, IEEE Transactions on Vehicular Technology 70 (8) (2021) 7908–7920. doi:10.1109/TVT.2021.3095194.